Second harmonic generation (SHG) imaging of cancer heterogeneity in ultrasound guided biopsies of prostate in men suspected with prostate cancer

Ling, Yuting; Li, Chunhui; Feng, Kairui; Palmer, Scott; Appleton, Paul L.; Lang, Stephen; McGloin, David; Huang, Zhihong; Nabi, Ghulam

Published in:
Journal of Biophotonics

DOI:
10.1002/jbio.201600090

Publication date:
2016

Document Version
Publisher's PDF, also known as Version of record

Wiley Online Library
Early View publication on www.wileyonlinelibrary.com
(issue and page numbers not yet assigned;
citable using Digital Object Identifier – DOI)

J. Biophotonics 1–8 (2016) / **DOI** 10.1002/jbio.201600090

Journal of BIOPHOTONICS

FULL ARTICLE

Second harmonic generation (SHG) imaging of cancer heterogeneity in ultrasound guided biopsies of prostate in men suspected with prostate cancer

Yuting Ling[**, 1, 2], *Chunhui Li*[**, 1, 2], *Kairui Feng*[2], *Scott Palmer*[1], *Paul L. Appleton*[3], *Stephen Lang*[4], *David McGloin*[2], *Zhihong Huang*[2], *and Ghulam Nabi*[*, 1]

[1] Academic Section of Urology, Division of Cancer Research, School of Medicine, University of Dundee, Dundee DD1 9SY, Scotland, UK
[2] School of Science and Engineering, University of Dundee, Dundee DD1 4HN, Scotland, UK
[3] Dundee Imaging Facility, School of Medicine, University of Dundee, Dundee, DD1 9SY, UK
[4] Department of Pathology, Ninewells Hospital, Dundee, DD1 9SY, UK

Received 8 April 2016, revised 13 July 2016, accepted 19 July 2016
Published online 23 August 2016

Key words: Prostate cancer (PCa), collagen, second harmonic generation (SHG), orientation, preferred orientation, Gleason score

Prostate cancer is a multifocal disease with characteristic heterogeneity and foci that can range from low grade indolent to aggressive disease. The latter is characterised by the well-established histopathological Gleason grading system used in the current clinical care. Nevertheless, a large discrepancy exists on initial biopsy and after the final radical prostatectomy. Moreover, there is no reliable imaging modality to study these foci, in particular at the level of the cells and surrounding matrix. Extracellular matrix (ECM) remodelling is significant in cancer progression with collagen as the dominant structural component providing mechanical strength and flexibility of tissue. In this study, the collagen assembly in prostate tissue was investigated with second harmonic generation (SHG) microscopy: malignant foci demonstrated a reticular pattern, with a typical collagen pattern for each Gleason score. The orientation of collagen for each biopsy was computed by applying a ratio of the anisotropic and isotropic collagen fibres. This value was found to be distinct for each Gleason score. The findings suggest that this approach can not only be used to detect prostate cancer, but also can act as a potential biomarker for cancer aggressiveness.

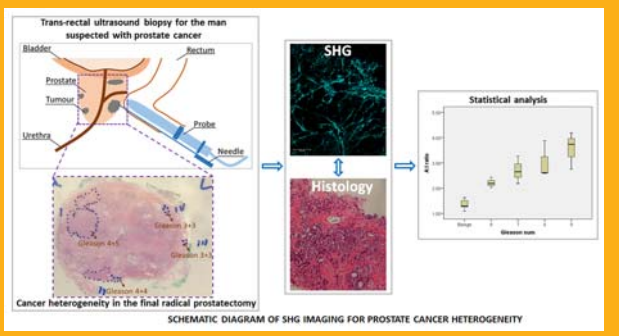

SCHEMATIC DIAGRAM OF SHG IMAGING FOR PROSTATE CANCER HETEROGENEITY

1. Introduction

Despite a number of recent advances in the diagnosis and staging of human prostate carcinomas (PCa), there has been a strong research focus on accurately characterising patients for whom treatment outcomes can be predicted. The need for this has been highlighted by the fact that over/under diagnosis remains a significant healthcare challenge in clinically localised disease [1, 2]. A large disparity exists between Gleason scores (the histological scoring system used to grade prostate cancer) [3] on initial

* Corresponding author: e-mail: g.nabi@dundee.ac.uk
** These authors contributed equally to this work.

biopsy and after the final radical prostatectomy. This may result in sub-optimal therapy. A more accurate method for determining disease status in the initial biopsy would enable more appropriate therapy choices to be made. It has been reported [4–8] that tissue stiffness measurement of prostate cancer can be used as a promising biomarker, both for the detection and characterisation of cancer foci. The stiffness of tissue is a result of increased cellularity and elevated collagen contents [9, 10].

There are two main cell types in the prostate gland: epithelia and stromal cells [11, 12]. The secretory epithelia in the normal human prostate gland are confined by the basement membrane and the surrounding stroma consists of the extracellular matrix (ECM), fibroblasts, smooth muscle cells (SMC), immune cells, nerves and blood vessels. Several studies [13–16] indicate that tumour stroma is different from the stroma in normal tissue. PCa cells proliferate and invade through the basement membrane into the host stroma followed by ECM remodelling and basement membrane degradation. The disruption creates a new stromal microenvironment termed 'reactive stroma' [14–16] to support cancer cell survival, proliferation and migration, and induce angiogenesis. In breast cancer [17, 18], remodelling and reorientation of collagen with multiple collagen fibres aligned perpendicular to the tumour boundary may vary with aggressiveness of cancer foci. For instance, straightening of aligned collagen fibres may promote intravasation. Therefore, techniques that identify and characterize features of the epithelial-stromal microenvironment are of great diagnostic potential and interest.

Second harmonic generation (SHG) imaging is a popular imaging tool for visualisation and characterisation of non centrosymmetric 3D structures such as collagen in medicine and biology [19–22]. It can obtain high-contrast 3D images of collagen fibres based on the variations in the ability of the sample to generate second-harmonic light. This imaging method is based on a nonlinear light-matter interaction mechanism where the light emitted from the sample is twice the frequency (half the wavelength) of the incident light. SHG microscopy is similar to other optical imaging methods and is limited by strong scattering and absorption by tissue, but it can provide high spatial resolution images noninvasively without biomarkers or ionizing radiation. Moreover, the experimental setup and imaging interpretation are feasible even for the cellular and molecular scale of collagen fibres [23, 24].

In the present study, the collagen assembly in prostate tissue was imaged with second harmonic generation (SHG) microscopy. The correlation between histology, prostate cancer heterogeneity and SHG imaging will be discussed quantitatively using Fourier transform second harmonic generation (FT-SHG) [25–29]. FT-SHG imaging involves extracting quantitative metrics through the application of spatial Fourier analysis on the images of collagen-based prostate biopsy tissues obtained from SHG microscopy. We investigated differences in stromal collagen fibers in normal and malignant prostate biopsies. A parameter (A : I ratio) was applied to compute the regularity in collagen fiber orientation and utilized to compare across different Gleason scores. The parameter is a ratio of the anisotropic and isotropic collagen fibres. It was intended to develop a quantitative biomarker to make the diagnosis of PCa more accurate.

2. Materials and methods

2.1 Human prostate biopsy

Ethical approval was granted by Tayside ethical committee (14/ES/0049). Informed consent was obtained from all the patients before their biopsy procedures for the reported study. The prostate biopsies were obtained using trans-rectal ultrasound (TRUS) guided needle biopsy in men suspected with PCa. Each biopsy was a circular core approximately 1 mm in diameter and 1–2 cm in length. The biopsy specimens were processed using a routine pathology protocol and reported by an experienced histopathologist blinded to the SHG results. The procedure included fixing with formalin, embedding in paraffin, sectioning with a microtome and staining with haematoxylin and eosin (H&E). After processing, the stained histologic section had a thickness of ~5 μm, and was mounted between a glass slide and coverslip. Although staining is not required for SHG imaging, it is necessary for the histopathologist to report the cancer aggressiveness and beneficial for this study to correlate SHG with the histopathological results from the same slide.

The aggressiveness of PCa is characterized by Gleason score/grade based upon the architectural pattern of the glands of the prostate tumour under the microscope [3, 30]. Each pattern has a corresponding Gleason grade of 1 to 5. Gleason 1 is the most well-differentiated tumour pattern whilst Gleason 5 is the least differentiated tumour pattern. A Gleason score ($n + m$) combines a primary grade (n) and a secondary grade (m), where n is the predominant pattern of the tumour (greater than 50% of the total pattern), and m is the next-most prevalent. Besides this, the term Gleason score can be assigned in the form of the final sum of n and m, called the Gleason sum. If the latter is presented, the number can range from 2 to 10, but in the current clinical care the lowest score given is Gleason 3 + 3 = 6 [30].

Generally, a higher Gleason score/grade means a more aggressive tumour and a worse prognosis.

Twenty-four core biopsies were randomly selected and imaged with the SHG microscope by an independent investigator without knowledge of histopathology. The biopsy specimens were categorised into two major groups based on the pathologic diagnosis: namely benign prostate tissue (6 core biopsies) and malignant PCa (18 core biopsies). The malignant PCa samples further contained 5 sub-groups according to varied Gleason score: 1) 3 + 3 in 3 core biopsies, 2) 3 + 4 in 4 core biopsies, 3) 4 + 3 in 5 core biopsies, 4) 4 + 4 in 3 core biopsies, 5) 4 + 5 in 3 core biopsies. The spectrum provided sufficient numbers to study cancer heterogeneity using SHG.

2.2 Multiphoton SHG microscopy

An upright Multiphoton microscope TCS SP8 MP (Leica) at Dundee Imaging Facility was utilized to image the histopathology slides. The tunable near-IR laser (Spectra-Physics InSight DeepSee) produced linearly polarized pulses spectrally centred at 880 nm. After spatially filtering and collimation, the beam was sent to the galvo-scanner. Incident light at 880 nm was focused onto the sample with a Leica HC PL Fluotar 10 × 0.3 NA objective. Due to the momentum conservation, SHG signal is especially directional and emitted mainly in the forward direction, being collected by a 0.9 NA condenser lens. The SHG signal was then filtered through a laser blocking filter (SP 680) and an SHG bandpass filter (440/20) and detected with a standard photomultiplier. The SHG laser power was adjusted to around 50 mW so that sufficient signal was obtained without any obvious damage to the sample. The transmitted light image was obtained from a 488 nm laser and collected in the forward transmitted light position using a 483/32 filter. A combination of z-stack and tile scan was used to acquire the whole area of the biopsy section automatically. Using identical settings, 12-bit images of 3352 × 3352 pixels were acquired using LAS X (Leica Application Suite X).

2.3 Image analysis of SHG images

We quantified the alignment of collagen fibres in each section using Fourier transform second harmonic generation (FT-SHG) adapted from the reported studies [23–29, 31]. The processing algorithms were developed in the Matlab platform (Matlab R2015b, the MathWorks). Using a 2D Fourier transform (FT), the image contents are decomposed into a superposition of harmonic functions (of different amplitudes and angles) along two axes, where the spatial frequency is the modulation in intensity in the image per unit distance. This method is to identify the quantitative parameters that represent the collagen orientation in the prostate biopsies through assessment of the spatial frequencies in an image using a 2D-FT. In a given plane, the direction the majority of fibers tend to align along is defined as the pre-

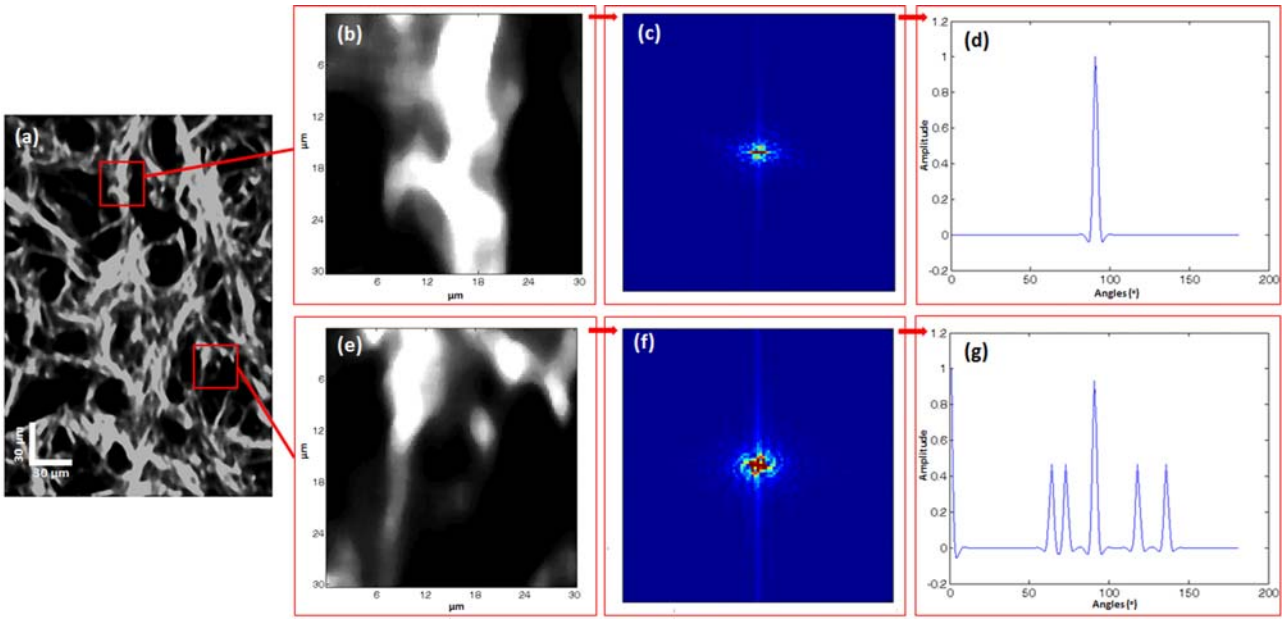

Figure 1 Imaging processing of SHG collagen in the malignant prostate biopsy. (**a**) Gray-scale image, typical (**b**) anisotropic and (**e**) isotropic collagen fibres after segmentation, 2D-FT images of the (**c**) anisotropic and (**f**) isotropic fibres, and the line plots of the orientation distribution of the (**d**) anisotropic and (**g**) isotropic fibres. Scale bar is 30 µm.

ferred orientation. In 2D-FT, the high amplitudes on average orient perpendicularly to the preferred orientation.

As shown in Figure 1a, the regions where collagen fibers had preferential orientation were labelled as anisotropic (Figure 1b) and regions with no preferential orientation (many different directions) were labelled as isotropic (Figure 1e). The 2D-FT images (Figure 1c and f) were created by applying fast Fourier transforms. It was integrated radially across different angles that resulted a plot of amplitude as a function of orientation angle. Gaussian fits were then applied to the plot. The center of the fit illustrated the orientation of fibers as displayed in Figure 1d, and the width of the fits was the measurement of the randomness by which the fibers were distributed. In the angular power spectrum, the desired signal was selected with over –20dB of the highest amplitude in order to exclude background noise. Based on the experimental observation and the literature [31], the anisotropic region was represented by no more than four peaks, while isotropic region resulted in multiple peaks (Figure 1g) at least five.

2.4 Orientation illustration in the core biopsy slide

To calculate the preferred orientation more quickly, the original image was firstly divided into sub-images as illustrated in Figure 2 and categorized into three groups: negligible, anisotropic, or isotropic. Negligible (NN) was defined if the SHG intensity in the area was low or nearly dark. The sub-images where collagen fibers had preferential orientation were labelled as anisotropic (AA) and sub-images with many different directions were labelled as isotropic (II). In Figure 2, NN is then marked with blue, while II orange, and the rest of them were illustrated with the preferred orientation. Lastly, the overall orientation of the collagen fibers in each entire biopsy was quantified by applying A:I ratio (the ratio of the number of anisotropic (AA) to isotropic (II) sub-images). The aim is to compute the regularity in collagen fiber orientation and compare it across the biopsy core samples of different Gleason score.

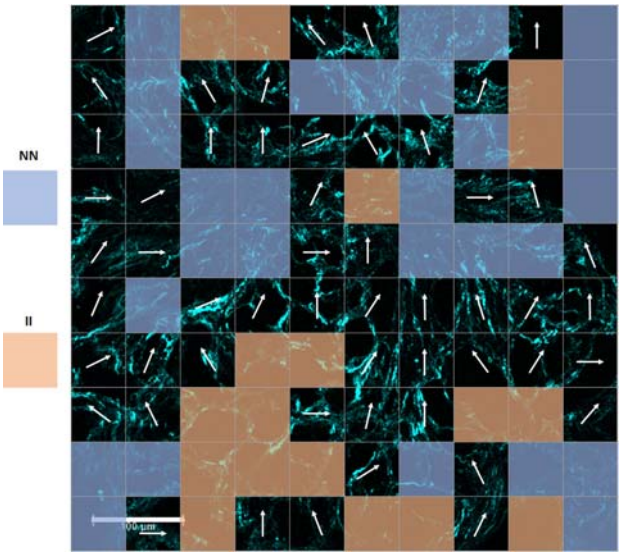

Figure 2 Sub-images analysis of collagen orientation in malignant prostate tissue. Dark or negligible (NN) ones are indicated in blue, and isotropic (II) ones are marked with orange. Scale bar is 100 μm.

3. Results

3.1 Normal prostate and malignant prostate cancer

The fibromuscular stroma is about half volume of the gland, and mainly consisted of smooth muscle and connective tissue. The H&E staining method is capable of depicting the tissue structure and cellular details, while the molecular structure in the ECM is missing. In this study, the H&E stained images were used as the reference standard. As shown in Figure 3c, the normal prostate is composed of a gland and surrounded stroma. The normal gland has a papillary projection view, and is confined by two layers

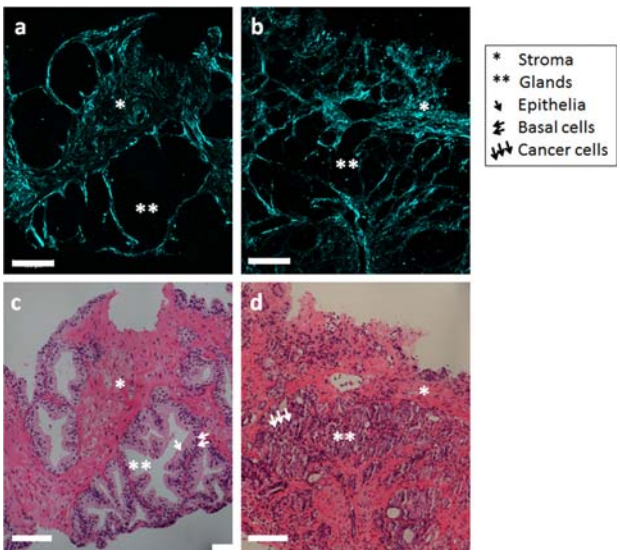

Figure 3 Comparison between benign and malignant prostate biopsy. SHG images of collagen alignment in (**a**) normal and (**b**) malignant prostate biopsy. Histological images of (**c**) normal glands and (**d**) fused glands occupied by cancer cells. Scale bar is 100 μm.

of cells. The inner layer is columnar epithelia and the outer layer is cuboidal basal cells. The epithelium is about two to four times of the height of the basal cell.

Figure 3a demonstrates that the SHG imaging provides the collagen distribution across the whole tissue. As epithelia or basal cells do not produce a detectable SHG signal, only the fibromuscular stroma is evident in the SHG channel with a substantial number of collagen fibers at different orientations. When cancer cells develop in the prostate, the basement membrane is lost and the epithelial layer is also disturbed. In some advanced cases of PCa, the cancer cells can even intrude into the stroma. By comparing Figure 3a and b, from normal to malignant prostate, the shape of the gland can change from papillary to reticular as the two layers that lined the gland are disrupted. In Figure 3b, the outlines of the glands are clearly observed to be fused together. The cancer cells are clustered and indicated by three arrows in Figure 3d. It is found that the collagen fibers tend to be more oriented in the malignant prostate biopsy in Figure 3b.

3.2 Characterization of Gleason pattern with SHG

Pathologically, the malignancy of PCa was categorized by Gleason score according to the cell pattern under the microscope. The higher the Gleason score, the more aggressive the cancer, and the worse the prognosis. To better understand prostate cancer progression, we imaged normal and cancerous biopsies using SHG, and compared the results with the Gleason score. Across all the samples in the SHG images in Figure 4a, the reticular pattern is observed as expected, but the size and shape vary from core to core and from region to region depending on tissue and cancer grade.

The SHG images (Figure 4a) are presented with the corresponding transmitted-light images (Figure 4b) from a 488 nm laser from the same imaging area. The transmitted-light images are similar to those from a conventional light microscope where the nuclei are blue and the cytoplasm and ECM are pink. The transmitted light detector produces a greyscale image in which the nuclei are dark and the rest of the tissue grey. Figure 4c fuses the SHG channel and transmitted light data.

For Gleason 3 + 3, the SHG signal between the glands is more than that in the higher grade of core biopsies. Also the margins of glands of Gleason 3 + 3 are still closed in shape, but these became fainter and even partially lost in Gleason 3 + 4 and 4 + 4. When the cancer is more aggressive, the cancer cells fill up the gland and some go into the stroma as well. The glands are fused together, and there are only sheets of cancer cells left in Gleason 4 + 5 with no glandular shape remaining. In SHG images, the different pattern of Gleason score can be distinguished by distribution and orientation of collagen fibrils.

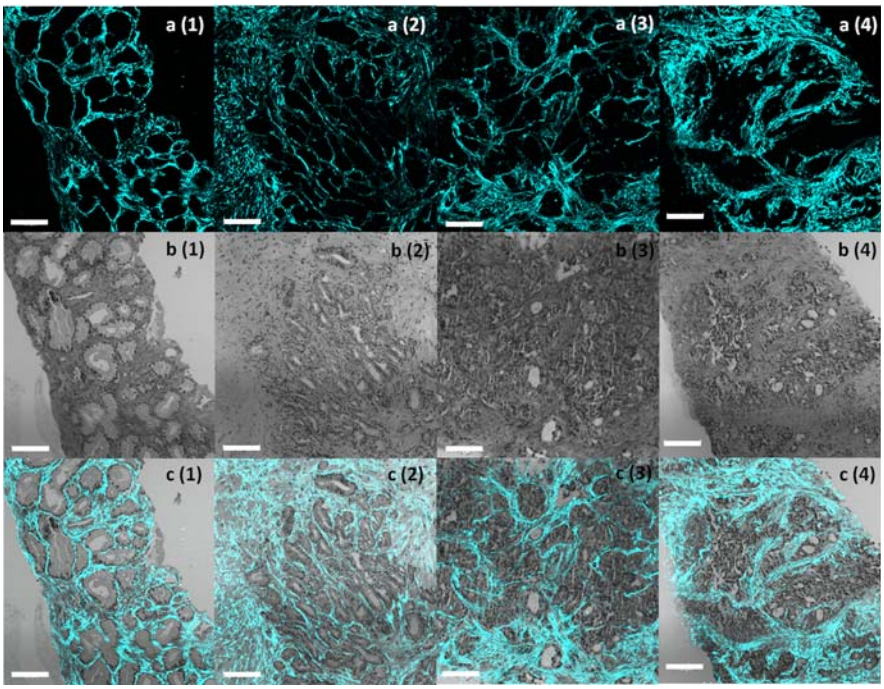

Figure 4 Core biopsies with increasing Gleason score. (**a**) SHG images, (**b**) transmitted-light images, (**c**) overlay images of Gleason 3 + 3(1), 3 + 4(2), 4 + 4(3), and 4 + 5(4), respectively. Scale bar is 100 μm.

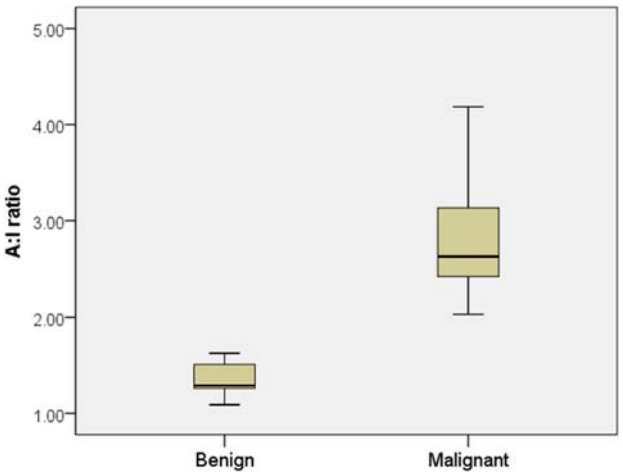

Figure 5 Whisker plot of the orientation between benign and malignant core biopsies.

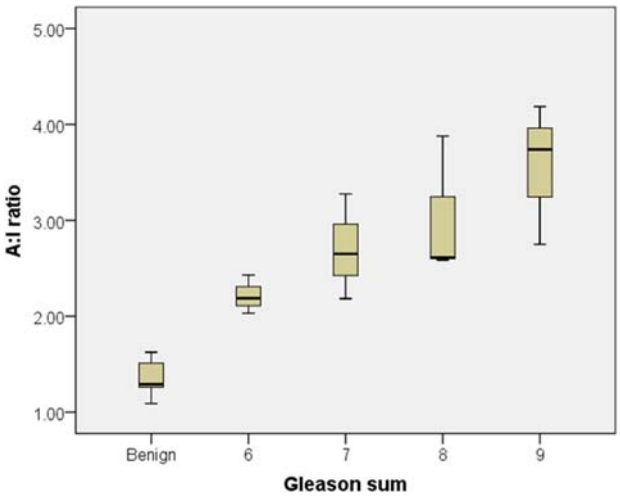

Figure 6 Whisker plot of the orientation (A : I ratio) among different Gleason sum.

3.3 Statistical analysis

To quantify the accuracy of the method described above, a systematic statistical analysis is also carried out for all the prostate core biopsies obtained in the study. As shown in Figure 5, the orientation (A : I ratio) of malignant samples is 2.82 ± 0.62, approximately twice that of benign samples (1.34 ± 0.19). Hence, the malignant samples have a higher degree of preferred alignment along a single direction compared to the normal ones. The *p*-value between benign and malignant biopsies is 0.043. Figure 6 displays a rising trend when the malignancy of the cancer increases. Among them, Gleason 9 is highly aligned, but the normal cores are almost isotropic. The mean value and the standard deviation of the normal biopsy and each Gleason score were demonstrated in Table 1.

4. Conclusions and discussion

PCa is a multifocal disease with characteristic heterogeneity and foci that can range from low grade indolent to aggressive disease. There have been a significant number of studies focused on accurately characterising patients using the Gleason score, and a large discrepancy exists on initial biopsy and after the final radical prostatectomy. Moreover, the pathophysiology, in particular the microenvironment of prostate cancer and the factors leading to its progression are not well understood. The prostate primarily consists of gland and stroma, and the latter is mainly a collection of collagen fibers which produce strong SHG signal.

SHG microscopy was utilized to compare the SHG images of normal and malignant prostate biopsies, and investigate those with different Gleason scores. All the samples were correlated with histological images using H&E staining, which is the golden standard for confirming presence or absence of prostate cancer. Note that epithelial layer and cancer cells are missing in the SHG images since they do not produce a detectable SHG signal. We found that collagen in malignant prostate cancer has a reticular instead of papillary pattern. However, the reticular pattern disappears in the highly advanced cancer such as Gleason 4 + 5. When the cancer cells are proliferating in an uncontrolled manner, the basement membrane is broken down, the glands are fused together and the cancer cells invade the gland and even the stroma. As a result, the SHG signal between glands is gradually lost.

Table 1 The comparison of Orientation among biopsy groups.

	Number of biopsy samples	Orientation (A : I ratio)	Minimum	Maximum
Benign prostate tissue	6	1.34 ± 0.19	1.09	1.63
Gleason score 3 + 3	3	2.22 ± 0.20	2.03	2.43
Gleason score 3 + 4	4	3.00 ± 0.27	2.65	3.28
Gleason score 4 + 3	5	2.46 ± 0.29	2.18	2.87
Gleason score 4 + 4	3	3.03 ± 0.74	2.59	3.88
Gleason score 4 + 5	3	3.56 ± 0.84	2.75	4.19

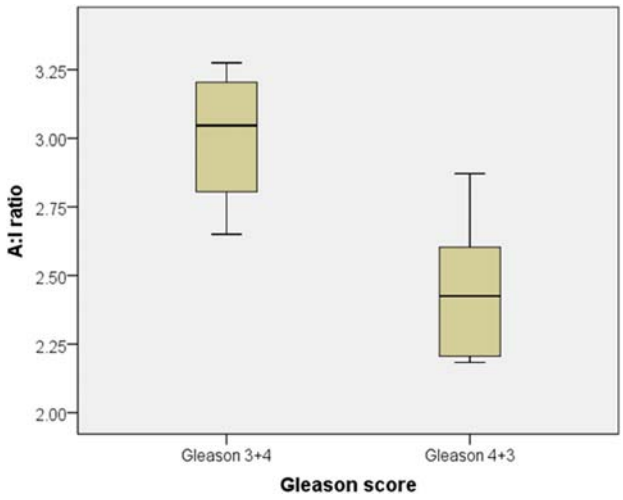

Figure 7 Whisker plot of the orientation (A : I ratio) between Gleason 3 + 4 and of Gleason 4 + 3.

Apart from morphologically different collagen patterns, we applied the FT-SHG to quantify the preferred orientation of collagen fibers in each biopsy. Generally, malignant cores are found to be more aligned than the normal ones. Besides, the higher the Gleason score, the larger the A : I ratio. It means that the collagen fibers tend to be more oriented as the prostate cancer becomes more aggressive. Note that there is a small fluctuation in the advanced grade of cancer in Figure 6. Among the groups, the value for the Gleason 8 is similar to Gleason 7. Moreover, as shown in Figure 7, Gleason 4 + 3 is more isotropic than Gleason 3 + 4 with a lower A : I ratio. However, it is still less anisotropic than Gleason 4 + 4 and 4 + 5 according to the Table 1.

The A : I ratio acquired from breast biopsies in [27] was 2.8 ± 1.5 for normal samples and 11.6 ± 6.7 for malignant ones. Both of them are at least twice the values obtained from the prostate biopsies. There could be several reasons for this discrepancy. The first is the nature of target tissue and the breast tissue is better differentiated in comparison to prostate tissue. Breast tissue contains much more collagen, and a different type of collagen structure could lead to a higher level of alignment. The second reason could be the FT-SHG method we utilized in this study is slightly different, such as the threshold, size of the sub-images, and resolution of the original images. Another possible reason is the sampling size of the study that is quite important in considering the differences. In this study, the sample diversity is limited as there were only twenty-four core biopsies in the study sample. To overcome the weakness, a future study with a larger sample number is necessary.

In summary, SHG provides high-resolution images of collagen distribution in prostate core biopsies. It is a noninvasive imaging method without the need for staining or ionizing radiation, but it can feasibly be applied to versatile types of biological samples with high-contrast morphological details of collagen fibers. Moreover, quantitative FT-SHG demonstrated that the A : I ratio can be used as a biomarker for diagnosis of PCa. There is significant potential to develop a systematic correlation between the Gleason score and the preferred orientation of the collagen fibers.

Acknowledgements The authors would like to acknowledge the financial support of Prostate Cancer UK (PCUK), the Scottish Universities Physics Alliance (SUPA) and EPSRC Grant no. EP/K503010/1. We appreciate the histopathological assistance from Stephen Lang, Department of Pathology, Ninewells Hospital, Dundee. The authors also thank the Dundee Imaging Facility, School of Life Sciences, University of Dundee for the use of equipment, advice and support.

Author biographies Please see Supporting Information online.

References

[1] R. M. Hoffman, New England Journal of Medicine **365**, 2013–2019 (2011).
[2] F. H. Schroder, J. Hugosson, M. J. Roobol, T. L. J. Tammela, M. Zappa, V. Nelen, M. Kwiatkowski, M. Lujan, L. Maattanen, H. Lilja, L. J. Denis, F. Recker, A. Paez, C. H. Bangma, S. Carlsson, D. Puliti, A. Villers, X. Rebillard, M. Hakama, U. H. Stenman, P. Kujala, K. Taari, G. Aus, A. Huber, T. H. van der Kwast, R. H. N. van Schaik, H. J. de Koning, S. M. Moss, A. Auvinen, and E. Investigators, Lancet. **384**, 2027–2035 (2014).
[3] J. I. Epstein J Urology **183**, 433–440 (2010).
[4] K. Hoyt, B. Castaneda, M. Zhang, P. Nigwekar, P. A. di Sant'Agnese, J. V. Joseph, J. Strang, D. J. Rubens, and K. J. Parker, Cancer biomarkers: section A of Disease markers **4**, 213–225 (2008).
[5] R. G. Barr, R. Memo, and C. R. Schaub, Ultrasound Q **28**, 13–20 (2012).
[6] S. Ahmad, R. Cao, T. Varghese, L. Bidaut, and G. Nabi, Surg Endosc. **27**, 3280–3287 (2013).
[7] S. Woo, S. Y. Kim, J. Y. Cho, and S. H. Kim, Korean J Radiol. **15**, 346–355 (2014).
[8] C. Li, G. Guan, Y. Ling, Y. T. Hsu, S. Song, J. T. Huang, S. Lang, R. K. Wang, Z. Huang, and G. Nabi, Cancer letters **357**, 121–128 (2015).
[9] M. H. Zaman, L. M. Trapani, A. L. Sieminski, D. Mackellar, H. Gong, R. D. Kamm, A. Wells, D. A. Lauffenburger, and P. Matsudaira, Proceedings of the National Academy of Sciences of the United States of America **103**, 10889–10894 (2006).
[10] J. Tang, Y. Zhang, M. B. Zhang, Y. M. Li, X. Fei, and Z. G. Song, Asian journal of andrology **16**, 305–308 (2014).

[11] A. Y. Liu and L. D. True, The American journal of pathology **160**, 37–43 (2002).
[12] P. Chiarugi, P. Paoli, and P. Cirri, Seminars in Oncology **41**, 267–280 (2014).
[13] C. Morrison, J. Thornhill, and E. Gaffney, Urological research **28**, 304–307 (2000).
[14] J. A. Tuxhorn, G. E. Ayala, and D. R. Rowley, The Journal of urology **166**, 2472–2483 (2001).
[15] J. A. Tuxhorn, G. E. Ayala, M. J. Smith, V. C. Smith, T. D. Dang, and D. R. Rowley, Clinical Cancer Research **8**, 2912–2923 (2002).
[16] D. A. Barron and D. R. Rowley, Endocrine-related cancer. **19**, R187–R204 (2012).
[17] P. P. Provenzano, K. W. Eliceiri, J. M. Campbell, D. R. Inman, J. G. White, and P. J. Keely, BMC Med. **4**(38), 1–15 (2006).
[18] M. W. Conklin, J. C. Eickhoff, K. M. Riching, C. A. Pehlke, K. W. Eliceiri, P. P. Provenzano, A. Friedl, and P. J. Keely, The American journal of pathology **178**, 1221–1232 (2011).
[19] P. Campagnola, Analytical chemistry **83**, 3224–3231 (2011).
[20] A. Keikhosravi, J. S. Bredfeldt, A. K. Sagar, and K. W. Eliceiri, Methods Cell Biol. **123**, 531–546 (2014).
[21] T. M. Bauman, T. M. Nicholson, L. L. Abler, K. W. Eliceiri, W. Huang, C. M. Vezina, and W. A. Ricke, PLoS ONE **9**, e109102 (2014).
[22] Y. Huang and Z. Zhuang, Scanning. **36**, 334–337 (2014).
[23] P. J. Campagnola, A. C. Millard, M. Terasaki, P. E. Hoppe, C. J. Malone, and W. A. Mohler, Biophysical journal **82**, 493–508 (2002).
[24] R. M. Williams, W. R. Zipfel, and W. W. Webb, Biophysical journal **88**, 1377–1386 (2005).
[25] R. A. R. Rao, M. R. Mehta, and K. C. Toussaint, Optics express **17**, 14534–14542 (2009).
[26] P. Matteini, F. Ratto, F. Rossi, R. Cicchi, C. Stringari, D. Kapsokalyvas, F. S. Pavone, and R. Pini, Optics express **17**, 4868–4878 (2009).
[27] R. Ambekar, T.-Y. Lau, M. Walsh, R. Bhargava, and K. C. Toussaint, Biomedical optics express **3**, 2021–2035 (2012).
[28] P. Matteini, R. Cicchi, F. Ratto, D. Kapsokalyvas, F. Rossi, M. de Angelis, F. S. Pavone, and R. Pini, Biophysical journal **103**, 1179–1187 (2012).
[29] R. Cicchi, D. Kapsokalyvas, M. Troiano, P. Campolmi, C. Morini, D. Massi, G. Cannarozzo, T. Lotti, and F. S. Pavone, Journal of biophotonics **7**, 914–925 (2014).
[30] J. I. Epstein, L. Egevad, M. B. Amin, B. Delahunt, J. R. Srigley, P. A. Humphrey, and G. Comm, Am J Surg Pathol. **40**, 244–252 (2016).
[31] R. Ambekar Ramachandra Rao, University of Illinois at Urbana-Champaign, 2012.